DOI 10.1007/s10717-023-00592-8
Glass and Ceramics, Vol. 80, Nos. 5 – 6, September, 2023 (Russian Original, Nos. 5 – 6, May – June, 2023)

UDC 666.3:544.6.018.42-16

$M_{0.9}Y_{0.1}O_{2-\delta}$–$BiScO_3$ (M = Zr, Ce) — PREPARATION, STRUCTURE, AND IONIC CONDUCTIVITY

I. V. Sudzhanskaya[1] and V. S. Sotnikova[1, 2]

Translated from *Steklo i Keramika*, No. 6, pp. 54 – 59, June, 2023.

Original article submitted March 2, 2023.

Samples of the solid solutions $Zr_{0.9}Y_{0.1}O_{2-\delta}$–$BiScO_3$ and $Ce_{0.9}Y_{0.1}O_{2-\delta}$–$BiScO_3$ were obtained by solid-phase synthesis. X-ray diffraction revealed that the system $Zr_{0.9}Y_{0.1}O_{2-\delta}$–$BiScO_3$ corresponds to a tetragonal structure with space symmetry group $P42/nmc$. The ceramic $Ce_{0.9}Y_{0.1}O_{2-\delta}$–$BiScO_3$ is two-phase and is characterized by a cubic structure with space symmetry group $Fm\bar{3}m$ and $Ia–3$. It was ascertained by means of impedance spectroscopy that the system $Ce_{0.9}Y_{0.1}O_{2-\delta}$–$BiScO_3$ has the highest electrical conductivity, but the activation energy is lower in the ceramic $Zr_{0.9}Y_{0.1}O_{2-\delta}$–$BiScO_3$, equal to 0.3 eV in the temperature range 420 – 680°C. The activation energy of the solid solution $Ce_{0.9}Y_{0.1}O_{2-\delta}$–$BiScO_3$ is equal to 1.0 eV.

Keywords: multicomponent ceramic system, microstructure, ionic conductivity, impedance spectroscopy, activation energy.

INTRODUCTION

Solid solutions based on zirconium and cerium dioxide are used in the manufacture of solid electrolytes for solid oxide fuel cells, electrochemical sensors, electronic devices, and so on [1 – 3].

Doping of zirconium dioxide and cerium with rare earth and alkali metals, such as Y, Sc, Ca, Sr, and others, increases the electrical conductivity of electrolytes [1, 4 – 8].

The high operating temperatures (800 – 1000°C) of solid electrolytes, such as $Zr_{0.9}Y_{0.1}O_{2-\delta}$, effect a number of disadvantages, namely: long start-up time, the need for expensive sealing materials, and high energy costs to heat the element to operating temperature [9, 10].

More over, the electronic conductivity through the electrolyte must be negligible in order to avoid higher voltage losses, oxygen leakage, and the possibility of a short circuit [11, 12].

Recently, researchers have shown great interest in multicomponent ceramic systems with an eye toward improving the low-temperature properties of the developed materials of solid electrolytes based on ZrO_2 and CeO_2 as well as expanding the range of their applications.

Bi_2O_3 stabilized with isovalent cations exhibits high conductivity at temperatures < 650°C, which is approximately two orders of magnitude higher than that of zirconium dioxide [13]. However, the material based on Bi_2O_3 is thermodynamically unstable in a reducing atmosphere [14]. The addition of stabilized Bi_2O_3 to zirconium and cerium dioxide increases conductivity at < 700°C and also improves thermodynamic stability [15, 16].

For example, the authors of [15] found that the ionic conductivity of the ceramic $ErBiO_{2-\delta}$–$YZrO_2$ (4.6×10^{-2} Sm/cm at 700°C) increased on account of the diffusion of oxygen ions in the $ErBiO_{2-\delta}$ phase.

An investigation of the $Er_{0.4}Bi_{1.6}O_3$–$Sm_{0.075}Nd_{0.075}Ce_{0.85}O_{2-\delta}$ multicomponent system is advanced in [16]. The introduction of the composition $Er_{0.4}Bi_{1.6}O_3$ into the $Sm_{0.075}Nd_{0.075}Ce_{0.85}O_{2-\delta}$ matrix leads to a decrease in the sintering temperature to 1150°C, and as a result a structure with a finer grain size and higher conductivity is formed compared to the system $Sm_{0.075}Nd_{0.075}Ce_{0.85}O_{2-\delta}$.

Stabilization of Bi_2O_3 by scandium oxide in multicomponent systems ZrO_2–$SrTiO_3$–$BiScO_3$ and $YZrO_2$–$SrTiO_3$–$BiScO_3$ is presented in [17, 18]. The presence of the component $SrTiO_3$ with the perovskite structure, which has dielectric properties with a 3.2 eV band gap [19], can lead to an increase in the resistance along the grain boundaries.

The problem of the present work was to compare the microstructure and electrical conductivity of the ceramic sys-

[1] Belgorod National Research University, Belgorod, Russia (e-mail: sudzhanskaya@bsu.edu.ru).
[2] V. G. Shukhov Belgorod State Technological University, Belgorod, Russia (e-mail: sotnikova_v@bsu.edu.ru).

0361-7610/23/0506-0250 © 2023 Springer Science+Business Media, LLC

tems $Zr_{0.9}Y_{0.1}O_{2-\delta}$–$BiScO_3$ and $Ce_{0.9}Y_{0.1}O_{2-\delta}$–$BiScO_3$ below 700°C.

EXPERIMENTAL RESULTS, EQUIPMENT, AND PROCEDURES

Samples of the compositions $0.8Zr_{0.9}Y_{0.1}O_{2-\delta}$–$0.2BiScO_3$ and $0.8Ce_{0.9}Y_{0.1}O_{2-\delta}$–$0.2BiScO_3$ were obtained in two stages. The first one consisted in obtaining $BiScO_3$. For this, the oxides Bi_2O_3 and Sc_2O_3, taken in stoichiometric ratio, were stirred in an agate mortar with the addition of ethyl alcohol for 1 h, and then dried at 100°C for 30 min. The resulting powder was annealed at 1250°C for 2 h. The next stage consisted in obtaining $Zr_{0.9}Y_{0.1}O_{2-\delta}$ and $Ce_{0.9}Y_{0.1}O_{2-\delta}$ from the precursors Y_2O_3, ZrO_2, and CeO_2, taken in stoichiometric ratio. The resulting $Zr_{0.9}Y_{0.1}O_{2-\delta}$ and $Ce_{0.9}Y_{0.1}O_{2-\delta}$ powders were mixed with $BiScO_3$ in the ratio 4 : 1, taken by weight. Next, the compositions with the addition of ethyl alcohol were stirred in an agate mortar for 2 h, dried then dried at 100°C for 30 min. The compaction of the powders in the form of 1 mm thick and 10 mm in diameter tablets was conducted by a biaxial pressing method. For the composition $0.8Zr_{0.9}Y_{0.1}O_{2-\delta}$–$0.2BiScO_3$, the pressure was 70 MPa; the composition $0.8Ce_{0.9}Y_{0.1}O_{2-\delta}$–$0.2BiScO_3$ was pressed at 25 MPa. The samples were fired at 1250°C for 1 h in an air atmosphere.

The phase composition of the obtained samples was determined by x-ray diffraction (Rigaku Ultima IV x-ray diffractometer). The microstructure and elemental composition of ceramic samples were studied using a Quanta 600 FEG scanning ion-electron microscope. The electrical conductivity was measured using a Novocontrol Concept 43 impedance spectrometer operating on alternating current.

RESULTS AND DISCUSSION

It was ascertained by means of x-ray phase analysis (Fig. 1) that the ceramic system $Zr_{0.9}Y_{0.1}O_{2-\delta}$–$BiScO_3$ is single-phase, possesses a tetragonal structure with space symmetry group $P42/nmc$, and crystal lattice parameters equal to $a = b = 3.6016$ Å, $c = 5.1056$ Å The ceramic $Ce_{0.9}Y_{0.1}O_{2-\delta}$–$BiScO_3$ has two phases and a cubic structure with space symmetry group $Fm\bar{3}m$ with crystal lattice parameters $a = b = c = 5.3649$ Å and Ia–3 with crystal lattice parameters $a = b = c = 9.9076$ Å, respectively.

SEM images of the cleavage faces of the samples of $Zr_{0.9}Y_{0.1}O_{2-\delta}$–$BiScO_3$ and $Ce_{0.9}Y_{0.1}O_{2-\delta}$–$BiScO_3$ are displayed in Fig. 2.

The obtained images of both solid solutions $Zr_{0.9}Y_{0.1}O_{2-\delta}$–$BiScO_3$ and $Ce_{0.9}Y_{0.1}O_{2-\delta}$–$BiScO_3$ demonstrate grain structure. The system $Zr_{0.9}Y_{0.1}O_{2-\delta}$–$BiScO_3$ with average grain size 1.017 μm is distinguished by the greatest homogeneity; the ceramic $Ce_{0.9}Y_{0.1}O_{2-\delta}$–$BiScO_3$ is characterized by the presence of grains of two types: (1) dark gray — according to elemental composition determination by means of SEM — corresponds to the system $Ce_{0.9}Y_{0.1}O_{2-\delta}$–$BiScO_3$ with the average size 0.62 μm, and (2) bright grains — differing in the smallest size (0.41 μm) — correspond to $BiScO_3$.

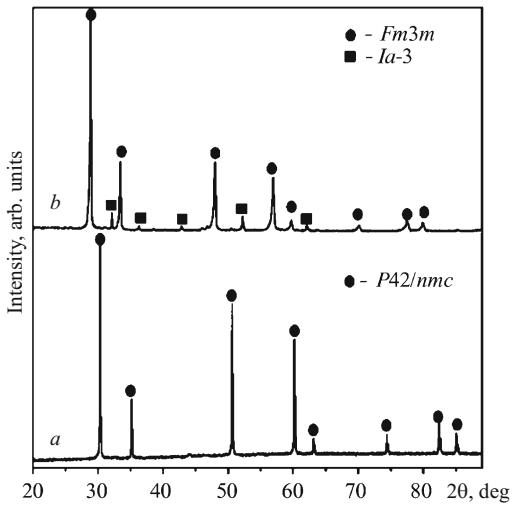

Fig. 1. X-ray diffraction patterns of the ceramic systems: *a*) $Zr_{0.9}Y_{0.1}O_{2-\delta}$–$BiScO_3$; *b*) $Ce_{0.9}Y_{0.1}O_{2-\delta}$–$BiScO_3$.

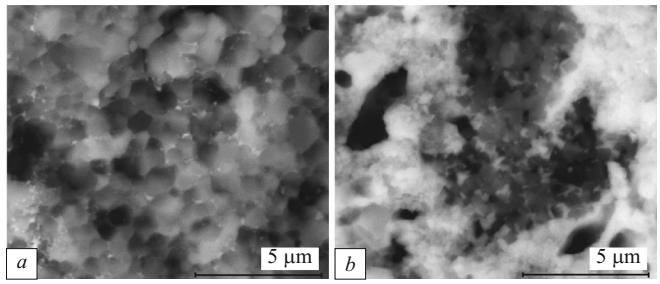

Fig. 2. SEM images of a cleavage of the ceramic systems: *a*) $Zr_{0.9}Y_{0.1}O_{2-\delta}$–$BiScO_3$; *b*) $Ce_{0.9}Y_{0.1}O_{2-\delta}$–$BiScO_3$.

The elemental composition of the samples and their percentage ratios were determined by means of energy dispersive analysis (EDS) of the ceramic systems $Zr_{0.9}Y_{0.1}O_{2-\delta}$–$BiScO_3$ and $Ce_{0.9}Y_{0.1}O_{2-\delta}$–$BiScO_3$ presented in Fig. 3.

The percentage weight fractions Wt of the elements in all samples are given in Table 1.

An analysis of the EMF results confirms the presence of the elements Y, Zr, Bi, Sc, Ce, and O in the two systems and the absence of other impurity elements, whose presence can result in specific conductivity reduction in the materials.

The temperature dependence of the electrical conductivity of the solid solutions systems $Zr_{0.9}Y_{0.1}O_{2-\delta}$–$BiScO_3$ and $Ce_{0.9}Y_{0.1}O_{2-\delta}$–$BiScO_3$ is determined by the dependence

$$\sigma = \sigma_0 e^{-\frac{E_a}{kT}}, \quad (1)$$

where σ_0 is an exponential factor; E_a is the activation energy;

TABLE 1. Elemental Weight Fractions Wt of the Synthesized Samples

Material	Element	Wt, %	Error, %
$Zr_{0.9}Y_{0.1}O_{2-\delta}BiScO_3$	O	36.73	10.75
	Sc	5.24	5.35
	Y	2.40	12.99
	Zr	51.45	3.43
	Bi	4.19	9.23
$Ce_{0.9}Y_{0.1}O_{2-\delta}BiScO_3$	O	7.19	0.47
	Y	18.27	0.25
	Bi	15.83	0.36
	Sc	5.04	0.36
	Ce	53.68	0.16

and k is Boltzmann's constant 1.38×10^{-23} J/K, and T is temperature, K (Fig. 4).

An analysis of the conductivity spectrum shows that the electrical conductivity is highest in the system $Ce_{0.9}Y_{0.1}O_{2-\delta}$–$BiScO_3$. This is associated with the large ionic radius of the cation Ce^{4+} (0.97 Å) compared to Zr^{4+} (0.84 Å) [20], so that a crystal structure with large conduction channels is formed [21, 22]. A sharp increase in the conductivity of the obtained ceramics is observed at 700 K, since the mobility of charge carriers increases with increasing temperature. To explain the mobility of charge carriers at different temperatures, the activation energy of the conduction process was calculated from the tangent of the slope angle of the function $\ln \sigma/(1/T)$ (inset in Fig. 4). For the system $Ce_{0.9}Y_{0.1}O_{2-\delta}$–$BiScO_3$ the activation energy in the range 300 – 680°C was equal to 1.0 eV. The solid solution is characterized by the presence of two straight line segments intersecting at the point 420°C (designated by an arrow on the graph). The activation energy of the system $Zr_{0.9}Y_{0.1}O_{2-\delta}$–$BiScO_3$ was equal to 0.3 eV in the 300 – 420°C and to 0.7 eV in the range 420 – 680°C.

In the low temperature range (300 – 420°C) the activation energy depends on two factors: the energy required to release charge carriers from complex defect associates and the energy required for the migration of oxygen vacancies. At lower temperatures the defects are coupled to one another and a large amount of energy is required to release oxygen vacancies from these defects. For this reason, at low operating temperatures, fewer mobile charge carriers are released, resulting in high activation energy and lower ionic conductivity. However, the enthalpy of association of defects began to decrease with increasing temperature, and an increasing number of charge carriers participate in the hopping mechanism. Therefore, the ionic conductivity is higher and the activation energy is lower.

In the system $Zr_{0.9}Y_{0.1}O_{2-\delta}$–$BiScO_3$ in our case an increase in the specific electrical conductivity and an increase in the activation energy are observed with increasing temperature, which could be associated with an increase in electronic conductivity.

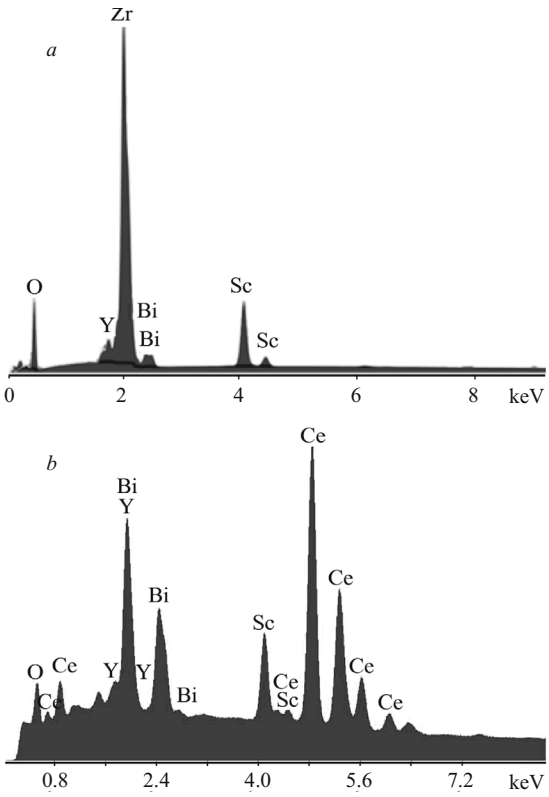

Fig. 3. Energy-dispersive spectra of ceramic systems: *a*) $Zr_{0.9}Y_{0.1}O_{2-\delta}$–$BiScO_3$; *b*) $Ce_{0.9}Y_{0.1}O_{2-\delta}$–$BiScO_3$.

CONCLUSIONS

Samples of the solid solutions $Zr_{0.9}Y_{0.1}O_{2-\delta}$–$BiScO_3$ and $Ce_{0.9}Y_{0.1}O_{2-\delta}$–$BiScO_3$ were obtained by solid-phase synthesis. With the aid of an x-ray diffractometer it was found that the system $Zr_{0.9}Y_{0.1}O_{2-\delta}$–$BiScO_3$ system has a tetragonal structure with the symmetry space group $P42/nmc$. The ceramic $Ce_{0.9}Y_{0.1}O_{2-\delta}$–$BiScO_3$ corresponds to a cubic structure with a space symmetry group $Fm\bar{3}m$ and Ia–3.

It was shown that the system $Zr_{0.9}Y_{0.1}O_{2-\delta}$–$BiScO_3$ with average grain size 1.017 μm is distinguished by the greatest homogeneity. The ceramic $Ce_{0.9}Y_{0.1}O_{2-\delta}$–$BiScO_3$ is characterized by the presence of grains of two types: (1) dark gray — corresponding to the system $Ce_{0.9}Y_{0.1}O_{2-\delta}$–$BiScO_3$ with an average grain size of 0.62 μm and (2) bright grains corresponding to $BiScO_3$ (average grain size 0.41 μm).

It was found by means of impedance spectroscopy that of the materials investigated the ceramic $Ce_{0.9}Y_{0.1}O_{2-\delta}$–$BiScO_3$ has the highest electric conductivity, but the activation energy is lower in the system $Zr_{0.9}Y_{0.1}O_{2-\delta}$–$BiScO_3$ amounting to 0.3 eV in the temperature range 300 – 420°C and 0.7 eV in 420 – 680°C. The activation energy of the solid solution $Ce_{0.9}Y_{0.1}O_{2-\delta}$–$BiScO_3$ is equal to 1.0 eV.

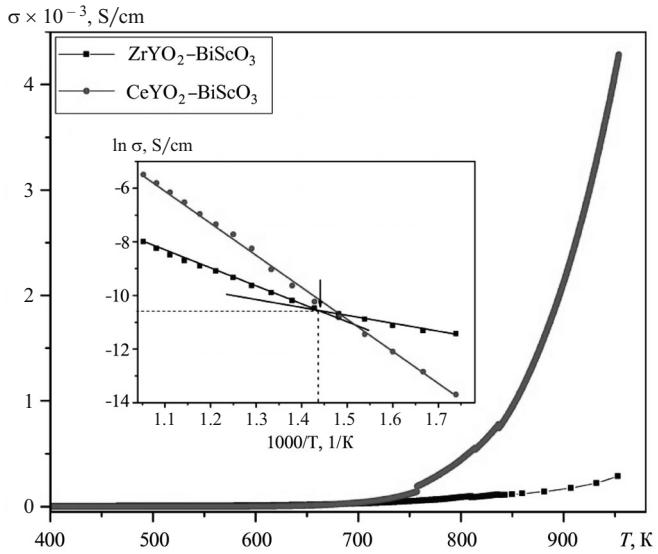

Fig. 4. Temperature dependence of the electrical conductivity of the ceramic systems $Zr_{0.9}Y_{0.1}O_{2-\delta}$–$BiScO_3$ and $Ce_{0.9}Y_{0.1}O_{2-\delta}$–$BiScO_3$.

This work was financially supported by the competitive part of the state assignment for the creation and development of laboratories, project No. FZWG-2020-0032 (2019-1569) using the equipment of the Center for Shared Use "Technologies and Materials of the National Research University "BelSU," as well as the Center for High Technologies of the V. G. Shukhov Belarusian State Technical University.

REFERENCES

1. J. Zhang, Ch. Lenser, N. H. Menzler, and O. Guillon, "Comparison of solid oxide fuel cell (SOFC) electrolyte materials for operation at 500°C," *Solid State Ionics*, **344**, 115 – 138 (2020).
2. S. Dwivedi, "Solid oxide fuel cell: Materials for anode, cathode and electrolyte," *Int. J. Hydrogen Energy*, **45**, 23988 – 24013 (2020).
3. E. L. Brosha, R. Mukundan, D. R. Brown, et al., "Development of ceramic mixed potential sensors for automotive applications," *Solid State Ionics*, **148**, 61 – 69 (2002).
4. B. Singh, S. Ghosh, S. Aich, and B. Roy, "Low temperature solid oxide electrolytes (LT-SOE): A review," *J. Power Sources*, **339**, 103 – 135 (2017).
5. D. W. Strickler and W. G. Carlson, "Ionic conductivity of cubic solid solutions in the system CaO–Y_2O_3–ZrO_2," *J. Am. Ceram. Soc*., **47**, 122 – 127 (1964).
6. J. H. Lee, S. M. Yoon, B. K. Kim, et al., "Electrical conductivity and defect structure of yttria-doped ceria-stabilized zirconia," *Solid State Ionics*, **144**, 175 – 184 (2001).
7. H. Inaba and H. Tagawa, "Review Ceria-based solid electrolytes," *Solid State Ionics*, **83**, 1 – 16 (1996). URL: https://doi.org/10.1016/0167-2738(95)00229-4
8. J. Kang, W. Feng, D. Guo, et al., "Performance optimization of Ca and Y co-doped CeO_2-based electrolyte for intermediate-temperature solid oxide fuel cells," *J. Alloys Comp*., **913**, 165 – 317 (2022). URL: https://doi.org/10.1016/j.jallcom.2022.165317
9. L. S. Mahmud, A. Muchtar, and M. R. Somalu, "Challenges in fabricating planar solid oxide fuel cells: A review," *Renewable and Sustainable Energy Rev.*, **72**, 105 – 116 (2017). URL: https://doi.org/10.1016/j.rser.2017.01.019
10. M. Irshad, K. Siraj, R. Raza, et al., "Description of high temperature solid oxide fuel cell's operation, materials, design, fabrication technologies and performance," *Appl. Sci*., **6**(3), 75 (2016). URL: doi.org/10.3390/app6030075
11. H. Shi, C. Su, R. Ran, et al., "Review. Electrolyte materials for intermediate-temperature solid oxide fuel cells," *Progr. Natural Sci.: Mater. Int*., **30**(6), 764 – 774 (2020). URL: https://doi.org/10.1016/j.pnsc.2020.09.003
12. S. Lubke and H. D. Wiemhofer, "Electronic conductivity of Gd-doped ceria with additional Pr-doping," *Solid State Ion*., **117**, 229 – 243 (1999). URL: https://doi.org/10.1016/S0167-2738(98)00408-1
13. P. Shu, H.-D. Wiemhöfer, U. Guth, et al., "Oxide ion conducting solid electrolytes based on Bi_2O_3," *Solid State Ionics*, **89**, 179 – 196 (1996). URL: https://doi.org/10.1016/0167-2738(96)00348-7
14. D. W. Joh, J. H. Park, D. Kim, et al., "Functionally graded bismuth oxide/zirconia bilayer electrolytes for high-performance intermediate-temperature solid oxide fuel cells (IT-SOFCs)," *ACS Appl. Mater. Interfaces*, **9**, 8443 – 8449 (2017). DOI: 10.1021/acsami.6b16660
15. D. W. Joh, J. H. Park, D. Y. Kim, et al., "High performance zirconia-bismuth oxide nanocomposite electrolytes for low temperature solid oxide fuel cells," *J. Power Sources*, **320**, 267 – 273 (2016).
16. L. Miao, J. Hou, K. Dong, and W. Liu, "A strategy for improving the sinterability and electrochemical properties of ceria-based LT-SOFCs using bismuth oxide additive," *Int. J. Hydrogen Energy*, **44**(11), 5447 – 5453 (2019). URL: https://doi.org/10.1016/j.ijhydene.2018.10.223
17. O. N. Ivanov, I. V. Sudzhanskaya, and M. N. Yapryntsev, "Manufacture, structure, and electric conductivity of ZrO_2–$SrTiO_3$–$BiScO_3$ ceramics," *Glass Ceram.*, **72**(11), 413 – 416 (2016). DOI: 10.1007/s10717-016-9800-4]
18. I. V. Sudzhanskaya, M. N. Yaprintsev, Yu. S. Nekrasova, et al. "Effect of $BiScO_3$ additive on the structure and electrical properties of the Y_2O_3–ZrO_2–$SrTiO_3$ system," *J. Nano- and Electronic Phys*., **11**(1), 01018 – 01022 (2019). DOI: 10.21272/jnep.11(1).01018
19. V. V. Deshmukh, C. R. Ravikumar, M. R. Anil Kumar, et al. "Structure, morphology, and electrochemical properties of $SrTiO_3$ Perovskite: Photocatalytic and supercapacitor applications," *Envir. Chem. Ecotoxic*., **3**, 241 – 248 (2021). URL: https://doi.org/10.1016/j.enceco.2021.07.001
20. R. D. Shannon, "Revised effective ionic radii and systematic studies of interatomic distances in halides and chaleogenides," *Acta Cryst*., **A32**, 751 (1976).
21. B. Singh, S. Ghosh, S. Aich, and B. Roy, "Low temperature solid oxide electrolytes (LT-SOE): A review," *J. Power Sources*, **339**, 103 – 135 (2017).
22. T.-H. Yeh and C.-C. Chou, "Ionic conductivity investigation in samarium and strontium co-doped ceria system," *Phys. Scr.*, **129**, 303 – 307 (2007). URL: https://doi.org/10.1088/0031-8949/2007/T129/067